# Electronic properties of ferrocenyl-terpyridine coordination complexes: An electrochemical and X-ray photoelectron spectroscopic approach

Ebrahiem Botha[a], Marilé Landman,[b] Peet H. van Rooyen[b] and Elizabeth Erasmus[a]*

[a] *Department of Chemistry, University of the Free State, Bloemfontein 9300, South Africa*

[b] *Department of Chemistry, University of Pretoria, Pretoria, South Africa.*

Contact author details:

Name: Elizabeth Erasmus

Tel: ++27-51-4019656

Fax: ++27-51-4017295

e-mail: erasmuse@ufs.ac.za

**TOC:**

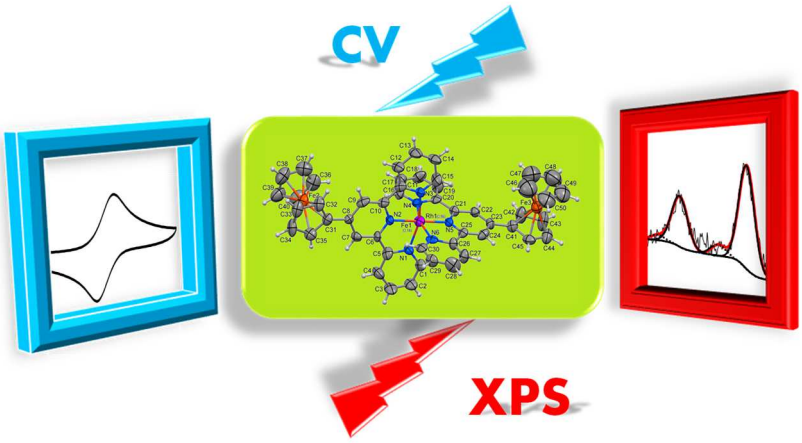


**Keywords:**

Ferrocenyl-terpyridine; electrochemistry; XPS; charge transfer; crystal structure

**Highlights**

- Preparation of coordinated ferrocenyl-terpyridine complexes
- Electrochemical study of the coordinated ferrocenyl-terpyridine complexes
- X-ray photoelectron spectroscopy of ferrocenyl-terpyridine coordination complexes
- The intensity of satellite structures in XPS indicated the amount of charge transferred
- Single crystal structure of $[Rh(Fctpy)_2][PF_6]_3$

## Synopsis

The electrochemical behavior of the $Fc/Fc^+$ of ferrocenyl-terpyridine coordination metal complexes is related to the charge transfer and binding energy of the Fe 2p photoelectron lines as measured by XPS, giving insight into the electronic properties of the complexes.


## Abstract

A series of 4'-ferrocenyl-2,2':6',2''-terpyridine coordination metal complexes, $[M(Fctpy)_2][PF_6]_x$ with M = Co (**2**), Fe (**3**), and Rh (**4**) and x = 2 (for **2** and **3**) or 3 (for **4**), was subjected to an electrochemical and X-ray photoelectron spectroscopic study. The formal reduction potential of the $Fc/Fc^+$ couple of the ferrocenyl-moiety ($Fe^{II}$) is related to the Allred Rochow electronegativities of the different coordinated metals, as well as with binding energies of the Fe $2p_{3/2}$ photoelectron lines (as measured by XPS).

The binding energy position of the main Fe $2p_{3/2}$ photoelectron line, spin-orbit splitting between the main and satellite structure (charge transfer band) of the Fe $2p_{3/2}$ photoelectron line as well as the intensity ratio between the of the main and satellite structure of the Fe $2p_{3/2}$ photoelectron line ($I_{ratio}$, this gives the relative amount of charge being transferred) gave insight in the electronic structure of these ferrocenyl-terpyridine coordination metal complexes, **2-4**.

A single crystal X-ray structure determination of **4** highlighted the disorder of the $PF_6$ counter anions as well as double occupancy of the central metal atom of Rh (in **4**) with Fe, the Fe:Rh ratio is 0.14:0.85.

## 1. Introduction

2,2':6',2''-Terpyridine is a tridentate ligand which contains three N-donor heterocyclic rings and its coordination chemistry is well documented.[1] The metal-ligand coordinative bond is characterised by its high strength and stability due to the strong d-π* back-donation, since terpyridines are an unusual strong π-acceptors (in comparison to other N-donors),[2] and due to the strong chelating effect.[3] The terpyridine ligand normally coordinates in a distorted octahedral geometry to transition metals forming a 6-coordinated metal complex.[4] Other coordination spheres and geometry have also been reported e.g. a 9-coordinated Eu(III) complex,[5] and the irregular 6-coordinated polyhedron coordinated complex of Hg(II).[6] The coordination complexes of terpyridines have applications in very diverse fields of research ranging from medicinal application (like anticancer and DNA intercalation) to material science (photovoltaics, sensitizers) and catalysis.[7, 8, 9, 10, 11, 12, 13, 14]

Substitution of terpyridine with different groups induces altered physical properties like variations in the electrochemical properties of the coordination complexes.[15, 16] It is well documented that electron withdrawing and donating substituents on ligands influence the oxidation and reduction potentials of the ligands and their metal complexes.[17, 18, 19, 20, 21, 22, 23] It would be interesting to determine if variation of the central coordination metals will display a similar effect on the electrochemical properties of the ligand, as having electron withdrawing and donating groups bound to the ligand. Since ferrocene and it derivatives has a predictable electrochemical behaviour of a one electron oxidation for the $Fc/Fc^+$ process, the ferrocenyl-substituted terpyridine ligand, 4'-ferrocenyl-2,2':6',2''-terpyridine, in its coordination complexes can be used to study the influence of the coordination metal on the electrochemical behaviour of the ferrocenyl-moiety.

X-ray photoelectron spectroscopy (XPS) is a quantitative and qualitative surface analysis technique based on the photoelectric effect.[24] This technique provides information on not only

the elemental composition, elemental dispersion and oxidation state of elements,[25] but also on the chemical environment surrounding each element (for a fixed oxidation state, the binding energy of the element increases as the electronegativity of the surrounding increases) and the electronic properties of the elements.[26]

The photoelectron lines of 3d transition metals in complexes, normally display satellite structures a few eV higher (due to a shake-up mechanism) or a few eV lower (due to a shake-down mechanism) than the main photoelectron lines as measured by the XPS. These substructures are universally accepted to be produced by the charge transfer from the ligand to the metal (which is known as a final state effect).[27, 28, 29, 30, 31, 32] Thus an in depth analysis of the XPS photoelectron lines and their substructure can also be used to enhance our insight on metal-ligand interactions and the electronic properties of the elements.[33, 34, 35, 36] The characterisation of terpyridine coordination complexes by means of XPS is underused.

In this paper we describe the preparation and characterisation of 4'-ferrocenyl-2,2':6',2''-terpyridine and its coordination complexes. The influence of the different coordination metals on the electrochemical behaviour of the ferrocenyl-moiety is described and related to the electronegativity of the coordination metal. An in-depth XPS investigation is described for the Fe 2p photoelectron lines and it substructure to gain insight into the electronic properties of these ferrocenyl-terpyridine coordination complexes.

## 2. Experimental

### 2.1. Synthesis

The ferrocenyl-terpyridine ligand was prepared according published procedures,[37] while the coordination metal complexes with M = $Co^{II}$, $Fe^{II}$, and $Rh^{III}$ were synthesised following a

modified procedure from Maity *et al.*[38] and Constable *et al.*[39] see the Supplementary Information for the detailed procedures.

### 2.2 Attenuated Total Reflectance Fourier Transform Infrared

Attenuated Total Reflectance Fourier Transform Infrared (ATR-FTIR) spectra were recorded from neat samples on a Digilab FTS 2000 Fourier transform spectrometer utilizing a He-Ne laser at 632.6 nm.

### 2.3. Electrochemistry

Cyclic voltammetry (CV) were recorded on a Princeton Applied Research PARSTAT 2273 Voltammographs, utilising Powersuite (version 2.58) software. A conventional three-electrode cell setup was used, with a platinum wire as the auxiliary electrode and the reference electrode was a silver wire, while the working electrode was a glassy carbon electrode which has a surface area 3.14 $mm^2$. The working electrode was polished on a Buhler polishing mat, utilising 1 micron and then ¼ micron diamond paste. Solutions contained 0.5 mM of analyte, 0.2 mM of decamethyl ferrocene as internal standard and 0.2 M tetrabutylammonium hexafluorophosphate as the supporting electrolyte and anhydrous acetonitrile as solvent. Temperatures were kept constant at 20 °C. All cited potentials were referenced against the $FcH/FcH^+$ couple as suggested by IUPAC [40]. Decamethylferrocene (Fc*, -0.610 V *vs.* $FcH/FcH^+$ under our experimental conditions) were used as internal standard.

### 2.4. X-ray photoelectron spectroscopy

XPS data was recorded on a PHI 5000 Versaprobe system, with a monochromatic Al Kα X-ray source. Spectra were obtained using the aluminium anode (Al Kα = 1486.6 eV) operating at 50 μm, 12.5 W and 15 kV energy (97 X-ray beam). The instrument work function was calibrated to give a binding energy of 284.8 eV for the lowest binding energy peak of the carbon 1s envelope, corresponding to adventitious carbon, which is not affected by neighbouring atoms. The spectra have been charge corrected to this main line of the C-C carbon 1s spectrum, of the adventitious carbon which was set to 284.8 eV. The survey scans were recorded at constant pass energy of 187.85 eV while the detailed region scans of C 1s, O 1s, P 2p, F 1s, N 1s, Fe 2p and the central metal's Co 2p and Rh 3d spectra was recorded at constant pass energy of 93.90 eV with the analyser resolution ≤ 0.5 eV. The resolution of the PHI 5000 Versaprobe system is FWHM = 0.53 eV at a pass energy of 23.5 eV and FWHM = 1.44 eV at a pass energy of 93.9 eV. The background pressure was 2 x $10^{-8}$ mbar. The XPS data was analysed utilising Multipak version 8.2c computer software,[41] and applying Gaussian–Lorentz fits (the Gaussian/Lorentz ratios were always >95%).

### 2.5. Crystal structure analysis

Data for the crystals, obtained from solutions in a mixture of ethanol and acetone, were collected on a Bruker D8 Venture kappa geometry diffractometer, with duo Iμs sources, a Photon 100 CMOS detector and APEX II control software,[42] using Quazar multi-layer optics monochromated, Mo-Kα radiation by means of a combination of ϕ and ω scans. Data reduction was performed using SAINT+[42] and the intensities were corrected for absorption using SADABS [i]. The structures were solved by intrinsic phasing using SHELXTS and refined by full-matrix least squares, using SHELXTL +[43] and SHELXL-2014+.[43] In the structure

refinements, all hydrogen atoms were added in calculated positions and treated as riding on the atom to which they are attached. All non-hydrogen atoms were refined with anisotropic displacement parameters; all isotropic displacement parameters for hydrogen atoms were calculated as X × Ueq of the atom to which they are attached, where X = 1.5 for the methyl hydrogens and 1.2 for all other hydrogens. Crystal data, data collection, structure solution and refinement details are available in CIF (CCDC deposit number 1558115).

## 3. Results and Discussion

### *3.1 Synthesis and characterisation*

The synthesis of the ferrocenyl-terpyridine, **1c**, starts with an aldol condensation between 2-acetyl pyridine and ferrocene-2-carboxalddehyde, **1a**, followed by a Michael addition of the second equivalent of 2-acetyl pyridine, to yield the ferrocenyl-1,5-diketone, **1b**. The ferrocenyl-1,5-diketone, **1b**, undergoes a ring closing reaction with ammonium acetate, resulting in the central pyridine ring, see **Scheme 1**. The reaction between the respective metal salt precursors ($Co(NO_3)_2$, $FeCl_2$, and $RhCl_3$) and the ferrocenyl-terpyridine, **1c**, in a 2:1 ligand to metal ratio in ethanol and subsequent precipitation with hexafluorophosphate afforded the coordinated ferrocenyl-terpyridine complexes, **2-4**.

Compounds **2** and **3** were isolated as the pure and intended compound. During the synthesis of **4** (the Rh derivative), a small amount (less than 8%) of the unintended complex $[Fe^{III}(Fctpy)_2][PF_6]_3$ was present. An attempt was made to prepare an Ir derivative from $IrCl_3$, but this afforded a mixture of two compounds, 9% of the intended Ir and 91% of $[Fe^{III}(Fctpy)_2][PF_6]_3$. The ligand, **1c**, is stable in solid form, however, in alcohol solutions even under inert atmosphere it is extremely light sensitive.[44, 45] During the reaction, the ligand decomposes to yield uncoordinated $Fe^{III}$ ions (resulting in a dark blue solution), which could

then also coordinate to **1c**, due to heating in EtOH and light exposure. This resulted in the formation unintended complex $[Fe^{III}(Fctpy)_2][PF_6]_3$, during the synthesis of **4** (the Rh derivative) and the Ir derivative. These can unfortunately not be separated, since recrystallization yielded a mixture of the intended and unintended products, which will be discussed in crystal structure segment. The Ir derivative will not be discussed further.

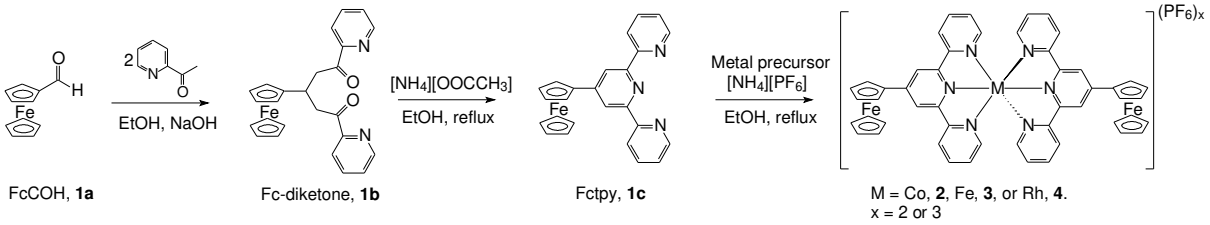


**Scheme 1.** The preparation of the ferrocenyl-terpyrdine ligand, **1c**, and the coordination complexes, **2-4**.

*3.2 Single Crystal X-ray structure of **4***

The perspective views of the molecular structure of **4** is shown in Figure 1, while the crystal data is summarized in the Supplementary Information. Selected bond lengths and angles may be found in Table 1.

The single crystal structure determination of **4** revealed that the metal atom is octahedrally coordinated and the structure include disordered $PF_6$ anions. Of significance is that this molecule contains both Rh and Fe in the same position, the refined ratio of their occupancy 0.857(12):0.143(12) for Rh:Fe. This double occupancy of the central atom occurs during the synthesis, as explained earlier. This structure included a $PF_6$ group in a general position, a $PF_6$ group on the symmetry position (inversion centre) and two partial, ill-defined and disordered

$PF_6$ groups. The contributions of these disordered $PF_6$ anions were linked to the refined occupancy factors of the central metal atom, as the Rh and Fe are in oxidation states 3 and 2 respectively, and were included in the refinement. The occupancy of the one anion group (labelled P3) refined to 0.714(7) and the second one (labelled P4) to 0.643(7).

As observed in a number of $[Fe(terpy)_2]^{2+}$ complexes the bite angle of the ligand deviates significantly from 180°, [44, 46] as reflected by the N-M-N' bond angles, around the central metal atoms which were found to be between 161.1 and 179.8°. This is in agreement with the reported range of 161.66 and 179.55° for similar iron terpyridine complexes.[44] The average M-N bond distances for **4** is 1.996 Å. As can be seen, the average Rh-N bond distance, in **4**, is slightly longer than that found in similar iron terpyridine complexes showing an average Fe-N bond length of 1.939 Å.[44, 45]

The C-C bond lengths of the ligands are between the typical ranges for carbon-carbon single bonds (1.54 Å) and carbon-carbon double bonds (1.337 Å),[47] indicating effective delocalization of the electrons in the ligand. This delocalization effect should be capable of transferring the electron donating effect of the ferrocenyl group of the ligand to the central metal as well as transferring the electronic properties of the central metal to the ferrocenyl group, which will be discussed in the electrochemical and XPS sections.

The average C-C bond distance for the cyclopentadienyl ring of the ferrocenyl-groups in **4**, is 1.419 and 1.423 Å for the substituted and unsubstituted cyclopentadienyl ring, respectively. The bond angles within the unsubstituted and the substituted cyclopentadienyl rings for the ferrocenyl-groups in **4** are ca. 108°, which is the theoretical value.

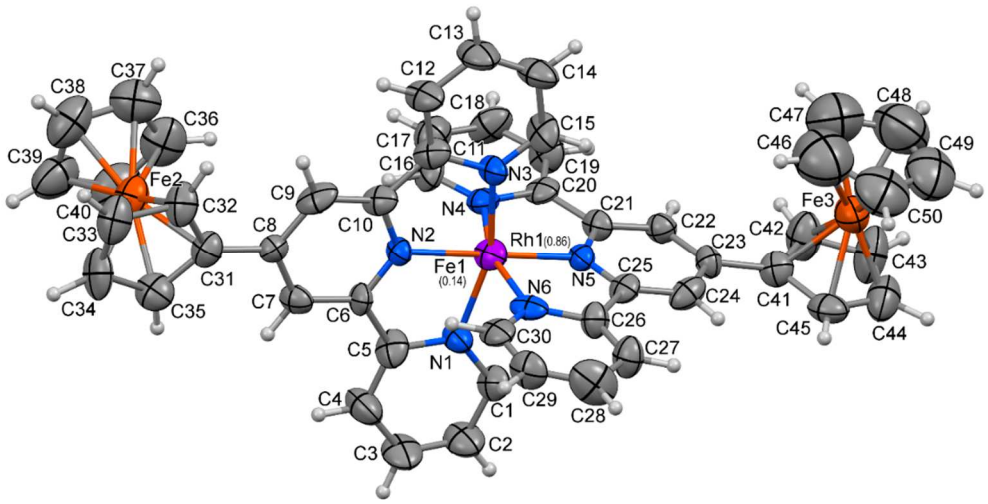


**Figure 1**. Molecular structure of $[Rh(Fctpy)_2][PF_6]_3$, **4**, showing atom labeling. The three $PF_6$ counter-ions, solvent molecules and hydrogens atoms have been omitted for clarity.

**Table 1.** Selected bond lengths (Å) and angles (°) for **4**. [M1 = Rh in **4**]

| **Bond distances / Å** | |
|---|---|
| **Atoms** | **4 (Rh/Fe)** |
| M1 - N1 | 2.020(10) |
| M1 - N2 | 1.945(9) |
| M1 - N3 | 2.027(9) |
| M1 - N4 | 2.020(10) |
| M1 - N5 | 1.934(9) |
| M1 - N6 | 2.027(9) |
| | |
| **Bond angles / °** | |
| **Trans N – M - N** | |
| N1 - M1 - N3 | 161.0(3) |
| N2 - M1 - N5 | 179.8(4) |

| | |
|---|---|
| N4 - M1 - N6 | 161.4(4) |
| | |
| **Cis N – M - N** | |
| N1 - M1 - N2 | 79.9(4) |
| N1 - M1 - N4 | 95.1(4) |
| N1 - M1 - N5 | 100.0(4) |
| N1 - M1 - N6 | 89.1(4) |
| N2 - M1 - N3 | 81.1(4) |
| N2 - M1 - N4 | 98.5(4) |
| N2 - M1 - N6 | 100.1(4) |
| N3 - M1 - N4 | 88.9(4) |
| N3 - M1 - N5 | 99.0(4) |
| N3 - M1 - N6 | 93.0(4) |
| N4 - M1 - N5 | 81.3(4) |
| N5 - M1 - N6 | 80.1(4) |
| | |
| **Dihedral angles / °** | |
| N1 - C5 - C6 - N2 | 5.2(15) |
| N2 - C10 - C11 - N3 | -4.1(15) |
| N4 - C20 - C21- N5 | -2.7(14) |
| N5 - C25 - C26 - N6 | -3.0(15) |

*3.3 FTIR and UV-Vis characterization*

The Fourier Transformed Infra-red spectra (FTIR) of **1b**, showed a strong $\nu_{CO}$ vibration at 1694 $cm^{-1}$. Upon ring closer which resulted in the ferrocenyl-terpyridine, **1c**, the $\nu_{CO}$ vibration disappeared, which allows for the monitoring of the ring closer reaction's progress. The $\nu_{CN}$ vibration of **1c** is observed at 1603 $cm^{-1}$, and upon coordination with the transition metals (Co, in **2**, Fe in **3** and Rh in **4**) a blue shift to ca. 1612 $cm^{-1}$ of the $\nu_{CN}$ vibration occurs. CH-stretching

frequencies are also observed between 3050-3200 $cm^{-1}$ for both the ligand, **1c**, and the complexes, **2-4**.

The maximum absorbance (molar absorptivity) of the bands measured by UV-Vis spectra of the ferrocenyl-terpyridine ligand, **1c**, and its metal complexes, **2-4**, is summarised in **Table 2** and the spectra are shown in **Figure 2**. The molar absorptivities, ε, of all the complexes **2-4** in acetonitrile solutions were relatively high. A linear relationship was obtained between the different concentrations and its measured absorbance for the ligand, **1c**, and all the complexes, **2-4** (see **Figure 2** insert, **4** is shown as an example). This implies that the Beer-Lambert law is being followed, A = ε Cl.

**Table 2.** Wavelengths at peak maxima ($\lambda_{max}$) and molar absorptivity, ε, of UV–Vis bands of **1c** and **2-4** in acetonitrile.

| Compound | Metal | $\lambda_{max}$ / nm (ε / $M^{-1}$ $cm^{-1}$) |
|---|---|---|
| **1c** | - | 458 (1086); 360 (2627); 314 (9840) |
| **2** | Co | 542 (15235); 356 (30000);321 (79176) |
| **3** | Fe | 587 (12846); 356 (5095); 322 (24285) |
| **4** | Rh | 584 (6820); 409 (13680); 331 (34660) |

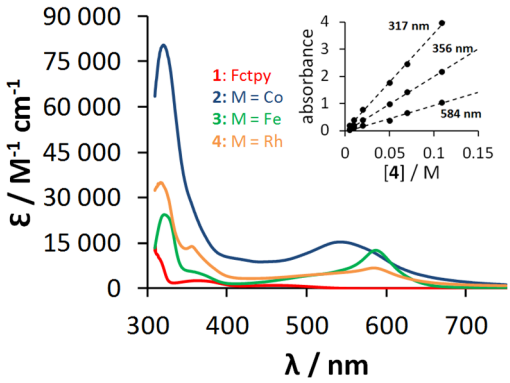

**Figure 2.** UV–Vis spectra of the ferrocenyl-terpyridine, **1c**, (red) and the $[M(Fctpy)_2][PF_6]_x$ complexes **2** (M = Co, x = 2; blue), **3** (M = Fe, x = 2; green), **4** (M = Rh, x = 3; orange), all in 0.5 mM solutions in acetonitrile. Insert: The linear relationship between the different concentration of **4** and its measured absorbance at λ = 317, 356 and 584 nm.

A distinctive band was observed at ca. 585 nm in the UV-Vis spectra in acetonitrile for **3-4**, with the exception of **2**, which showed this band at 542 nm. The ferrocenyl-terpyridine ligand, **1c**, does not show this band. When the ferrocenyl-terpyridine, **1c**, coordinates to a transition metal, the energy of the π* orbital decreases, which then gives rise to the charge transfer band observed for the coordinated complexes, **2-4**. Thus, this band at ca. 585 nm for **3-4**, and 542 nm for **2** is assigned to a ligand-to-metal charge transfer. This is in agreement with published results of similar complexes in a 50% water/DMF solution (Fe-complex, 590 nm; Co-complex, 543 nm).[38]

*3.4 Electrochemistry*

The electrochemical activity of the ferrocenyl-moiety within the ferrocenyl-terpyridine ligand, **1c**, and the coordinated complexes, **2-4**, was investigated by means of cyclic volammetry (CV) in an acetonitrile/tetrabutylammonium hexafluorophosphate solvent system. The CV's of the uncoordinated ferrocenyl-terpyridine ligand, **1c**, at different scan rates and different switching potentials are shown in **Figure 3** Left with selected data summarised in **Table 3**. The ferrocenyl-terpyridine ligand, **1c**, shows a chemically and electrochemically irreversible oxidation wave, $O_1$ at $E^{0'}$ = 0.696 V with $i_{pc}/i_{pa} \approx 0.4$ and ΔE = 0.276 V ($E_{pa}$ = 0.834 V) vs $FcH/FcH^+$. It also reveals four chemically and electrochemically irreversible reduction waves, $R_1$ to $R_4$ (see **Figure 3** Left), below -1 V vs $FcH/FcH^+$. The first reduction process, $R_1$, observed

at -1.424 V seems to be connected to the oxidation wave, $O_1$. When the switching potential for the CV scan of **1c** is set at 0.46 V, which is before the oxidation, $O_1$, the reduction process, $R_1$, is not observed. However, when the switching potential is set at 1.56 V, after the oxidation, $O_1$, the reduction process, $R_1$, is observed. Very small re-oxidation peaks are observed for $R_1$ to $R_4$, which increases in intensity as the scan rate increases, implying that a small amount of the reduced species of **1c** (which probably has a very short life-span) gets re-oxidised within the time-span of the CV experiment. The reduction peaks, $E_{pc}$, of the reduction waves $R_2$ to $R_4$ were observed at -1.749, -1.993 and -2.547 V vs $FcH/FcH^+$, respectively. The oxidation wave marked $O_1$ as well as the reduction waves marked $R_1$ to $R_4$ are assignable to the oxidation and reduction of the terpyridine moiety. This allocation is analogue with published data of a related ligand, bipyridine, which also showed an oxidation wave above 1.5 V and a number reduction processes below -2 V vs $FcH/FcH^+$.[48]

The $Fc/Fc^+$ redox couple of **1c** was found to be a chemical and electrochemical reversible couple with the $i_{pc}/i_{pa} \approx 1$ and $\Delta E = 0.09$ mV. The $E^{0'}$ value of the ferrocenyl-terpyridine, **1c**, was found to be 0.50 V vs $FcH/FcH^+$, which corresponds with the published values. The formal electrode potentials (vs SCE) of ferrocenyl-terpyridine derivatives (were the Fc is connected to the terpyridine by different spacers) was reported to be between 0.52 and 0.57 V.[49]

The comparative CV's of the $Fc/Fc^+$ redox couple of the uncoordinated ligand, **1c**, and the coordinated complexes **2-4** are shown in **Figure 3** Right, while the comparative CV's showing the entire potential window are provided in the Supplementary Information Figure S1 and selected data are summarised in **Table 3**.

The ferrocenyl-moiety within the ferrocenyl-terpyridine of the coordinated complexes, **2-4**, revealed a chemical and electrochemical reversible oxidation wave ($i_{pc}/i_{pa} \approx 0.95$ and $\Delta E \approx$ 0.085 mV), with the Rh coordination complex, **4**, having a slightly larger $\Delta E$ of 0.1 mV. The

slight larger ΔE of complexes **4**, could be explained by the double occupancy of the central metal as determined from the crystal structure. Since there are two different complexes within the mixture, the intended Rh (**4**) and the unintended $Fe^{III}$ derivative, the ΔE is a combination of both redox couples of complexes **4** and $[Fe^{III}(Fctpy)_2][PF_6]_3$, resulting in a slight larger ΔE than expected.

The $E^{0'}$ value of the Fe redox process of the ferrocenyl-terpyridine coordination complexes, **2-4**, differ only slightly from each other with an overall variation of 0.024 V (see **Table 3**). The order of increasing $E^{0'}$ values of the $Fc/Fc^+$ couple is Rh; **4** (0.097 V) < Fe; **3** (0.117 V) < Co; **2** (0.121 V). This order of increasing $E^{0'}$ values is related to the Allred Rochow electronegativity[50] of the coordinated transition metal (see **Table 3**), as the electronegativity of the central coordination metal increases the formal reduction potential of the ferrocenyl-moiety of the ferrocenyl-terpyridine ligand also increases. As the electron density moves towards the centre of the complex, it becomes increasingly more difficult to remove an electron (oxidise) from the ferrocenyl-moiety. The "directly proportional" relationship implies good electronic communication through the bonds of the coordinated complex, as predicted by the crystal structure data showing the delocalised electrons over the bonds. However, the influence of different central metals is not as big as when there are different R-groups (with a variation in electronegativity) attached within a ligand for instance ferrocenyl-chalcones,[51, 52] *p*-substituted phenyl diphenylphospinite ligand and their Rh-complexes,[22, 53] porhyrins,[34] β-diketonato ligands and their complexes.[23, 54]

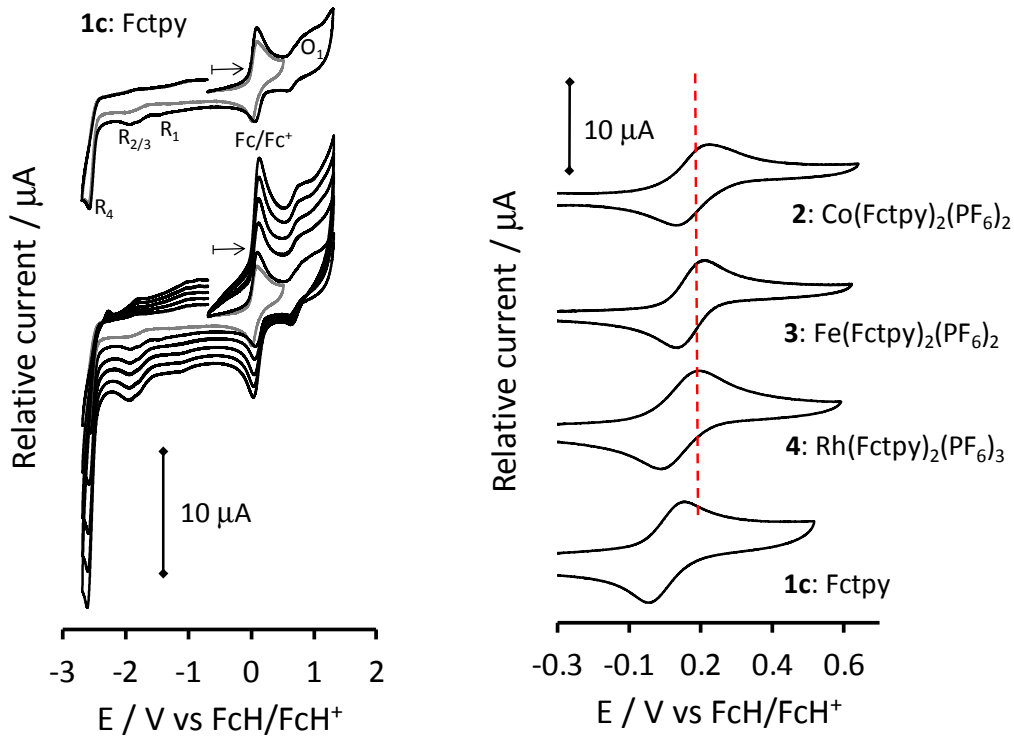


**Figure 3**. Left bottom: The cyclic voltammograms at scan rates of 0.1 (smallest current), 0.2, 0.3, 0.4 and 0.5 V $s^{-1}$ of the ferrocenyl-terpyridine, **1c**, referenced vs $FcH/FcH^+$. Left top: The CV of **1c** at 0.1 V $s^{-1}$ with a switching potential of 0.46 V (grey line) and 1.56 V (black line). Right: The comparative CV's of the $Fc/Fc^+$ redox couple of ca. 0.5 mM solutions of **1c**, and **2-4**, at a scan rate of 0.1 V $s^{-1}$ in an acetonitrile/tetrabutylammonium hexafluorophosphate solvent system measured at 20 ºC and referenced vs $FcH/FcH^+$. The dashed red line is set at 0.147 V to indicate the shift in oxidation potentials of the other metal complexes.

**Table 3.** Selected electrochemical data of the uncoordinated ferrocenyl-terpyridine ligand, **1c**, as well as the coordination complexes **2-4** at a scan rate of 0.1 V $s^{-1}$. All cited potentials are in V and referenced against the $FcH/FcH^+$ couple.

| | Metal | Allred Rochow electronegativity | $E_{pa}$ / V | ΔE / V | $E^{0'}$ / V | $i_{pc}/i_{pa}$ |
|---|---|---|---|---|---|---|
| **1c** | - | - | 0.095 | 0.090 | 0.050 | 0.98 |
| **2** | Co | 1.70 | 0.192 | 0.082 | 0.151 | 0.90 |
| **3** | Fe | 1.64 | 0.163 | 0.081 | 0.123 | 0.91 |
| **4** | Rh | 1.45 | 0.144 | 0.100 | 0.094 | 0.95 |

*3.5 X-ray photoelectron spectroscopy*

To further characterise the uncoordinated ferrocenyl-terpyridine ligand **1c** and the coordinated complexes, **2-4**, X-ray Photoelectron Spectroscopy (XPS) measurements was collected of these complexes. XPS is normally used for the characterisation of solid surface to determine the elemental composition and chemical states of the elements. XPS measures the core level binding energies of the elements under investigation, which are sensitive towards the chemical environment of the element. Elements under the influence of an electron withdrawing environment will display binding energies at higher eV, while element in an electron donating environment will have binding energies at lower eV than the standard expected binding energy position of the elements in a specific oxidation state.[24] XPS is very powerful characterization technique to probe the electronic environment of a complex, since (in addition to the oxidation state and chemical environment) it gives information of the charge transfer, amount of charge transfer, charge transfer energy and inner sphere reorganisation.

Similar to the electrochemical investigation, the XPS will only focus on the ferrocenyl-moiety, however, all the other elements (C, O, N, P, F and Co (for **2**), Rh (for **4**)) were detected by the XPS. The maximum binding energy of the main photoelectron line of the carbon, C 1s, of the adventitious carbon within carbon-carbon bonds was set at 284.8 eV, and this was used as an "internal reference" to charge correct the binding energies of the other elements for accurate comparison. The N 1s photoelectron line of the nitrogen of the terpyridine-moiety in the

uncoordinated ligand, **1c**, was detected at 398.53 eV and at ca. 399.3 eV for the coordinated complexes, **2-4**. The maximum binding energy of the P 2p envelope of the hexafluorophosphate counter ion was located at 135.8 eV while the F 1s was found at ca. 685.6 eV for **2-4**. The binding energies of the coordinated central metal atoms are: **2**, Co $2p_{3/2}$ = 780.19 eV (confirming that in the coordination complex Co is $Co^{II}$, in analogue with reported data of $Co^{II}$ located between 780 and 781 eV);[55, 56] **3**, Fe $2p_{3/2}$ = 708.24 eV (indicating the Fe is in the II oxidation state according to reported data of $Fe^{II}$ being located at ca. 708 eV);[57] **4**, Rh $3d_{5/2}$ = 309.90 eV (confirming the presence of $Rh^{III}$ normally located at ca. 310 eV).[58] The correct atomic ratio between the different elements was obtained, confirming the correct complexes was prepared, for **2**, a ratio of 1:5.9:1.9:1.8:11.6 for Co:N:Fe:P:F was obtained (expected ratio is 1:6:2:2:12), and for **3**, a ratio of 3:6.7:2.1:12.6 for Fe:N:P:F was obtained (expected ratio is 3:6:2:12). For complex **4**, more Fe than expected was measure. Complex **4** showed ca. 40% more Fe than expected, which is attributed to the mixture of the crystal of **4** and the unintended $[Fe^{III}(Fctpy)_2][PF_6]_3$. This 40% excess of Fe shows that there is a ratio of 1:0.13 between **4** and $[Fe^{III}(Fctpy)_2][PF_6]_3$ , which has 3 Fe atoms, one centre and two ligands, similar to what was obtained by the crystal structure determination.

The comparative XPS data of the ferrocenyl-terpyridine, **1c**, and the coordination complexes, **2-4**, with respect to the Fe 2p regions is presented in **Figure 4** and **Table 4**. The binding energy at the peak maximum of the Fe $2p_{3/2}$ photoelectron lines ($BE_{main\ Fe2p3/2}$) of **1c** were observed at 710.38 eV while $BE_{main\ Fe2p3/2}$ for **2-4** are located ca. 707.12 eV (varying with the different coordination metals). There is a binding energy difference between of ca. 3.3 eV between the $BE_{main\ Fe2p3/2}$ of the ferrocenyl-terpyridine ligand, **1c**, and the coordinated complexes **2-4**. This dramatic decrease in binding energy upon coordination is attributed to the lowering of the energy of the π* orbital, which is also responsible for the appearance of the charge transfer band observed in the UV-Vis spectra.

The observed $BE_{main\ Fe2p3/2}$ for the complexes **2-4** correlates well with the reported $BE_{main\ Fe2p3/2}$ values for ferrocene (707.8 eV)[59], ferrocenyl-containing chalcones (707.7 eV),[60, 61] and Fc/Ag(100) (707.9 eV).[62] This binding energy is, however, lower than the $BE_{main\ Fe2p3/2}$ reported for ferrocenyl-containing β-diketones and their Mn complexes (708.2),[36, 63] ferrocenyl-moiety linked via an aminoalkyl silane onto silicon (709.7 eV),[64] and $Fe^{II}$ in metal hexacyanoferrate (708.0 eV).[65] A spin orbit splitting of ca. 12.7 eV was obtained between the main Fe $2p_{3/2}$ and Fe $2p_{1/2}$ photoelectron lines ($\Delta BE_{main} = BE_{main\ Fe2p1/2} - BE_{main\ Fe2p3/2}$). A satellite peak (caused by the shake-up mechanism) at ca. 4.7 eV higher than the main Fe $2p_{3/2}$ photoelectron lines was also observed in the XPS spectra.

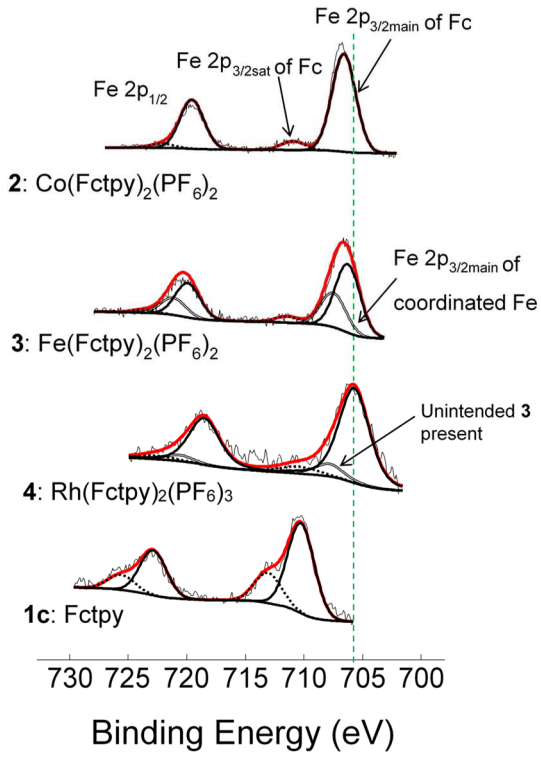


**Figure 4**. Comparative XPS spectra showing peak simulated fittings for the main Fe 2p and satellite Fe 2p peaks for ligand **1c**, and complexes **2-4**. The dashed green line is set at 706.88 eV to indicate the shift in BE of the other metal complexes.

The binding energy of an element is influenced by its chemical environment, implying if it experiences an electron withdrawing (causing an increase in BE) or electron donating (causing a decrease in BE) environment. It has been reported that an increase in the Gordy group electronegativity of varying R-groups within a ligand (β-diketonato ligand) directly increases the BE of the central metal and other element within the complex.[33, 35, 66]

The Allred Rochow electronegativity of the different coordination metals in the complexes **2**-**4**, again has an influence on the binding energy position of the main Fe $2p_{3/2}$ photoelectron line. As the Allred Rochow electronegativity (ARE) of the different coordination metals increases advancing from complex **4** to **3** and eventually to **2**, an increase in the binding energy of the main Fe $2p_{3/2}$ photoelectron line is observed Rh; **4** (ARE = 1.45; Fe $2p_{3/2\ main}$ = 706.15 eV) < Fe; **3** (ARE = 1.64; Fe $2p_{3/2\ main}$ = 707.15 eV) < Co; **2** (ARE = 1.70; Fe $2p_{3/2\ main}$ = 707.47 eV). As a result of the increased Allred Rochow electronegativity of the different coordination metals, electron density moves away from the ferrocenyl-moiety, causing the Fe $2p_{3/2}$ photoelectron line, to appear at higher binding energies.

The shake-up satellite peaks detected at a binding energy of ca. 4.7 eV higher than the main Fe 2p photoelectron lines, are associated with charge transfer,[67] from the terpyridine-moiety to the ferrocenyl-moiety. Due to the influence of the varying coordination metals in the center of the complexes, the amount of charge being transferred from the terpyridine-moiety to the ferrocenyl-moiety is not the same for the different complexes. A smaller charge transfer peak is indicative of less charge (electron density) being transferred to the ferrocenyl-moiety relative to the larger charge transfer peak. To quantify the amount of charge transferred, the ratio of the intensities (% area) of the charge transfer peak to the intensity of the main Fe $2p_{3/2}$ photoelectron line is used. This ratio is given by $I_{ratio} = (I_{Fe\ 2p3/2\ CT})/(I_{Fe\ 2p3/2\ main})$.[63] The amount

of charge transferred is again a result of the Allred Rochow electronegativity (ARE) of the different coordination metals. The general trend as indicated in **Table 4**, shows that the more electron density being pulled away from the ferrocenyl-terpyridine ligand by the coordination metal (as indicated the a higher ARE), the less charge is being transferred from the terpyridine-moiety to the ferrocenyl-moiety (as indicated by $I_{ratio}$). This result is in agreement with reported data for three different metal-dihalides series, $MnX_2$, $FeX_2$ and $CoX_2$,[68] with X = F, Cl or Br, where the $I_{ratio}$ increased as the Pauling electronegativity,[69] of the halides decreased.

The above mentioned three series of metal-dihalides also showed an increased trend of the separation between the maximum binding energies of the satellite and the main metal M $2p_{3/2}$ peaks, $\Delta BE = BE_{M2p3/2sat} - BE_{M2p3/2main}$, with increasing electronegativity of the halides, also referred to as charge transfer energy (CTE).[70] This CTE is the apparent energy needed to transfer one electron from the 2p state of the ligand to the 3d state of the metal. The amount of CTE is dependent on the electronegativity of the ligand. It has been reported that as the electronegativity of the ligand increases the CTE also increases.[70, 71] However, in this study the CTE (as calculated from $CTE = \Delta\ BE_{Fe2p3/2sat\ -\ Fe2p3/2main} = BE_{Fe2p3/2sat} - BE_{Fe2p3/2main}$) from the terpyridine-moiety to the ferrocenyl-moiety shows an inversely proportional correlation to the Allred Rochow electronegativity of the different coordination metals (see **Table 4**), which opposite to the expected. This implies that as the coordination metal's ARE increases the energy required for the transfer of one electron decreases. This opposite to the expected trend could possibly be attributed to the fact that the CTE of the ligand (as measure by the Fe 2p) is correlated to electronegativity of the central coordination metal and not the other way around as in the reported examples.

**Table 4**. Allred Rochow electronegativity of the coordination metals. The maximum binding energies of the main and satellite Fe $2p_{3/2}$ and Fe $2p_{1/2}$ photoelectron lines, the spin orbit

splitting of maximum binding energies of the Fe 2p photoelectron lines, $\Delta$ $BE_{main}$ and $\Delta$ $BE_{sat}$, the charge transfer energy (CTE) as well as, the % area ratio between main Fe $2p_{3/2}$ and the satellite Fe $2p_{3/2}$, $I_{ratio}$.

| | Metal | Allred Rochow E-neg | $BE_{main\ Fe\ 2p3/2}$ / eV | $BE_{main\ Fe\ 2p3/2}$ / eV | $\Delta BE_{main}$ / eV | $BE_{sat\ Fe\ 2p3/2}$ / eV | $BE_{sat\ Fe\ 2p3/2}$ / eV | $\Delta BE_{sat}$ / eV | $I_{ratio}$ | CTE / eV |
|---|---|---|---|---|---|---|---|---|---|---|
| **1c** | - | - | 710.38 | 722.90 | 12.52 | 707.55 | 720.17 | 12.62 | 0.34 | 2.83 |
| **2** | Co | 1.70 | 707.47 | 720.05 | 12.58 | 711.68 | 722.51 | 10.83 | 0.085 | 4.21 |
| **3** | Fe | 1.64 | 707.15 | 719.72 | 12.57 | 711.82 | 723.17 | 11.35 | 0.09 | 4.67 |
| **4** | Rh | 1.45 | 706.88 | 719.67 | 12.79 | 712.25 | 722.5 | 10.25 | 0.13 | 5.37 |

During the electrochemical oxidation of the ferrocenyl-moiety of ferrocenyl-terpyridine, **1c**, and its coordination complexes, **2-4**, electrons are removed from the iron ($Fe^{II}$), creating a $Fe^{III}$ positively charged species. When the ferrocenyl-terpyridines, **1c**, and **2-4**, are being irradiated with X-rays during the XPS experiment, core electrons get emitted, also generating positively charge species. Considering that both electrochemistry and photoionization creates positively charge species, it is expected that a link should exist between the binding energies of the main Fe 2p photoelectron lines and the formal redox potentials ($E^{o'}$) of the ferrocenyl-groups in complexes **1c** and **2-4**. The general trend shows that, the more difficult it is to remove an electron electrochemically, the more difficult it is to emit a core electron by photoionization:

Rh; **4** ($E^{o'}$ = 0.097 V; Fe $2p_{3/2\ main}$ = 706.15 eV) < Fe; **3** ($E^{o'}$ = 0.117 V; Fe $2p_{3/2\ main}$ = 707.15 eV) < Co; **2** ($E^{o'}$ = 0.121 V; Fe $2p_{3/2\ main}$ = 707.47 eV).

## 4. Conclusion

During the synthesis an unintended product, $[Fe^{III}(Fctpy)_2][PF_6]_3$, formed which could not be separated from **4** resulting in a 0.86:0.14 Rh:Fe mixture.

The formal reduction potentials ($E^{o'}$) of the $Fc/Fc^+$ couple of the ferrocenyl-terpyridine ligand within the coordination complexes **2-4** are directly proportional to the Allred Rochow electronegativity of the different coordination metals. Deconvolution of the Fe 2p photoelectron lines of the XPS and its charge transfer peaks (satellite peaks at a few eV higher than the main photoelectron line) gave better insight into the electronic structure of the ferrocenyl-terpyridine coordination complexes **2-4**.

The intensity and position of the charge transfer peaks (satellite structures) of the Fe 2p photoelectron lines are related to the amount of charge transferred between the terpyridine-moiety of the ligand and the ferrocenyl-moiety of the ligand.

## Conflicts of interest

There are no conflicts of interests to declare.


## Acknowledgements

The work has received financial support from the NRF (South Africa) and the central research fund of the UFS and UP.


## Supporting Information

Crystallographic data for **4**. The cif file of **4** contains all the supplementary crystallographic data for this paper. This material is available free of charge via the Internet from the Cambridge

Crystallographic Data Centre, 12, Union Road, Cambridge CB2 1EZ, UK; fax: +44 1223 336033, CCDC 1558115, http://www.ccdc.cam.ac.uk/conts/retrieving.html).


[1] J.A.G. Williams, Chem. Soc. Rev. 38 (2009) 1783.

[2] A. Czap, F. W. Heinemann, R. van Eldik, Inorg. Chem. 43 (2004) 7832.

[3] H. Hofmeiera, U.S. Schubert, Chem. Soc. Rev. 33 (2004) 373.

[4] K. Lashgari, M. Kritikos, R. Norrestam, T. Norrby, Acta Crystallogr., Sect. C: Cryst. Struct. Commun. 55 (1999) 64.

[5] N.S. Baek, Y.H. Kim, D.H. Lee, K.D. Seo, H.K. Kim, Bull. Korean Chem. Soc. 30 (2009) 1553.

[6] D. Matkovid-Calogovid, Z. Popovid, B. Korpar-Cofig, J. Chem. Crystallogr. 25 (1995) 453.

[7] K. Mitra, U. Basu, I. Khan, B. Maity, P. Kondaiah, A.R. Chakravarty, Dalton Trans. 43 (2014) 751.

[8] A. Winter, G.R. Newkome, U.S. Schubert, Chem. Cat. Chem. 3 (2011) 1384.

[9] G.R. Whittell, M.D. Hager, U.S. Schubert, I. Manners, Nat. Mater. 10 (2011) 176.

[10] A. Wild, A. Winter, F. Schlatter, U.S. Schubert, Chem. Soc. Rev. 40 (2011) 1459.

[11] I. Eryazici, C.N. Moorefield, G.R. Newkome, Chem. Rev. 108 (2008) 1834.

[12] A. Winter, M. Gottschaldt, G.R. Newkome, U.S. Schubert, Curr. Top. Med. Chem. 11 (2011) 5864.

[13] H.J. Park, K.H. Kim, S.Y. Choi, H.M. Kim, W.I. Lee, Y.K. Kang, Y.K. Chung, Inorg. Chem. 49 (2010) 7340.

[14] G.C. Vougioukalakisa, T. Stergiopoulosa, G. Kantonisa, A.G. Kontosa, K. Papadopoulosa, A. Stubllab, P.G. Potvinb, P. Falaras, J. Photochem. Photobiol. A: Chem. 214 (2010) 22.

[15] S. Romain, C. Baffert, C. Duboc, J.C. Lepretre, A. Deronzier, M.N. Collomb, Inorg. Chem. 48 (2009) 3125.

[16] N. Yoshikawa, T. Matsumura-Inoue, Anal Sci. 19 (2003) 761.

[17] W.C. du Plessis, J.J.C. Erasmus, G.J. Lamprecht, J. Conradie, T.S. Cameron, M.A.S. Aquino, J.C. Swarts, Can. J. Chem. 77 (1999) 378.

[18] J. Conradie, T.S. Cameron, M.A.S. Aquino, G.J. Lamprecht, J.C. Swarts, Inorg. Chim. Acta 358 (2005) 2530.

[19] J. Conradie, J.C. Swarts, Dalton Trans. 40 (2011) 5844.

[20] E. Erasmus, J. Conradie, A. Muller, J.C. Swarts, Inorg. Chim. Acta 360 (2007) 2277.

[21] M.S. Ram, L.M. Jones, H.J. Ward, Y. Wong, C.S. Johnson, P. Subramanian, J.T. Hupp, Inorg. Chem. 30 (1991) 2928.

[22] E. Erasmus, J. Electroanal. Chem. 727 (2014) 1.

[23] E. Erasmus, J.C. Swarts, New J. Chem. 37 (2013) 2862.

[24] J.W. Niemantsverdriet, Spectroscopy in Catalysis, Edition 3, John Wiley & Sons, Weinheim, 2007.

[25] E. Desimoni, B. Brunetti, Chemosensors 3 (2015) 70.

[26]J. Yarwood, R. Douthwaite, S. Duckett, Spectroscopic Properties of Inorganic and Organometallic Compounds: Techniques, Materials and Applications, Volume 41, RCS publishing, Cambridge, 2010.

[27] S. Asada, S. Sugano, J. Phys. Soc. Jpn. 41 (1976) 1291.

[28] S. Larsson, J. Electron Spectrosc. Relat. Phenom. 8 (1976) 171.

[29] S. Larsson, Chem. Phys. Lett. 40 (1976) 362.

[30] S. Larsson, M. Braga, Chem. Phys. Lett. 48 (1977) 596.

[31] T.A. Carlson, Photoelectron and Auger Spectroscopy, Plenum: New York, 1976.

[32] B. Feuerbacher, B. Fitton, R.F. Willis, Photoemission and the Electronic Properties of Surfaces, Wiley, New York, 1978.

[33] R. Lui, J. Conradie, E. Erasmus, J. Electron Spectrosc. Relat. Phenom. 206 (2016) 46.

[34] A. van As, C.C. Joubert, B.E. Buitendach, E. Erasmus, J. Conradie, A.N. Cammidge, I. Chambrier, M. J. Cook, J. C. Swarts, Inorg. Chem. 54 (2015) 5329.

[35] M.M. Conradie, J. Conradie, E. Erasmus, Polyhedron 79 (2014) 52.

[36] B.E. Buitendach, E. Erasmus, M. Landman, J.W. Niemantsverdriet, J.C. Swarts, Inorg Chem. 55 (2016) 1992.

[37] B. Farlow, T.A. Nile, J.L. Walsh, A.T. McPhail, Polyhedron 12 (1993) 2891.

[38] B. Maity, S. Gadadhar, T.K. Goswami, A.A. Karande, A.R. Chakravarty, Dalton Trans. 40 (2011) 11904.

[39] E.C. Constable, M.J. Hannon, A.J. Edwards, P.R. Taithby, J. Chem. Soc. Dalton Trans. (1994) 2669.

[40] G. Gritzner, J. Kuta, Pure Appl. Chem. 56 (1984) 461.

[41] F. Moulder, W.F. Stickle, P.E. Sobol, K.D. Bomben, Handbook of X-ray Photoelectron Spectroscopy, ULVAC-PHI, Inc., Enzo, Chigasaki, Japan, 1995.

[42] APEX2 (including SAINT and SADABS); Bruker AXS Inc., Madison, WI, 2012.

[43] G. M. Sheldrick, A short history of SHELX, Acta Cryst. A64 (2008) 112. DOI: 10.1107/S0108767307043930

[44] A. C. Benniston, D. Sirbu, C. Turta, M. R. Probert, W. Clegg, Tetra. Lett. 55 (2014) 3777.

[45] E. C. Constable, A. J. Edwards, R. Martinez-Manez, P. R. Taithby, A. M. W. Cargill Thompson, J. Chem. Soc. Dalton Trans. (1994) 645.

[46] E.C. Constable, C.E. Housecroft, M. Neuburger, D. Phillips, P.R. Raithby, E. Schofield, E. Sparr, D.A. Tocher, M. Zhender, Y. Zimmermann, J. Chem. Soc., Dalton Trans. (2000) 2219.

[47] R.C. Weast, Handbook of Chemistry and Physics, 63th edn., The Chemical Rubber Co., Ohio, pp. F180–F181.

[48] H. Ferreira, M.M. Conradie, K.G. von Eschwege, J. Conradie, Polyhedron 122 (2017), 147.

[49] U. Siemeling, J. Vor der Bruggen, U. Vorfeld, B. Neumann, A. Stammler, H.G. Stammler, A. Brockhinke, R. Plessow, P. Zanello, F. Laschi, F.F. de Biani, M. Fontani, S. Steenken, M. Stapper, G. Gurzadyan, Chem. Eur. J. 9 (2003) 2819.

[50] A.L. Allred, E.G. Rochow, J. Inorg. Nuclear Chem. 5 (1958) 264.

[51] E. Erasmus, Inorg. Chim. Acta 378 (2011) 95.

[52] T.J. Muller, J. Conradie, E. Erasmus, Polyhedron 33 (2012) 257.

[53] E. Erasmus, Polyhedron 106 (2016) 18.

[54] E. Erasmus, A.J. Muller, U. Siegert, J.C. Swarts, J. Organomet. Chem. 821 (2016) 62.

[55] C.V Schenck. J.G Dillard, J.W. Murry, J. Coll. Interf. Sci. 95 (1983) 398.

[56] D.L. Crowther. J.G. Dillard, Geochim. Cosmochim. Acta 47 (1983) 1399.

[57] N. Gauthier, G. Argouarch, F. Paul, M.G. Humphrey, L. Toupet, S. Ababou-Girard, H. Sabbah, P. Hapiot, B. Fabre, Adv. Mater. 20 (2008) 1952.

[58] E. Erasmus, Inorg. Chim. Acta 451 (2016) 197.

[59] J.A. Connor, L.M.R. Derrick, I.H.J. Hillier, J. Chem. Soc. 70 (1974) 941.

[60] E. Erasmus, S. Afr. J. Chem. 70 (2017) 94.

[61] E. Erasmus, J. Elec. Spec. Rel. Phen. 223 (2018) 84.

[62] C.M. Woodbridge, D.L. Pugmire, R.C. Johnson, N.M. Boag, M.A. Langell, J. Phys. Chem. B 104 (2000) 3085.

[63] B.E. Buitendach, E. Erasmus, J.W. Niemantsverdriet, J.C. Swarts, Molecules 21 (2016) 1427.

[64] M. Trzebiatowska-Gusowska, A. Gagor, E. Coetsee, E. Erasmus, H.C. Swart, J.C. Swarts, J. Organomet. Chem. 745 (2013) 393.

[65] S.J. Gerber, E. Erasmus, Mat. Chem. Phys. 203 (2018) 73.

[66] J. Conradie, E. Erasmus, Polyhedron 119 (2016) 142.

[67] J.S.H.Q. Perera, D.C. Frost, C.A. McDowell, J. Chem. Phys. 72 (1980) 5151.

[68] J. Park, S. Ryu, M. Han, S.J. Oh, Phys. Rev. B 37 (1988) 10867.

[69] L. Pauling, J. Amer. Chem. Soc. 54 (1932) 3570.

[70] A.J. Nelson, J.G. Reynolds, J.W. Roos, J. Vac. Sci. Technol. A 18 (2000) 1072.

[71] A.P. Grosvenor, B.A. Kobe, M.C. Biesinger, N.S. McIntyre, Surf. Interf. Anal. 36 (2004) 1564.